Astron. Astrophys. 324, 1190–1196 (1997)

ASTRONOMY
AND
ASTROPHYSICS

The first three-dimensional reconstruction of a celestial object at radio wavelengths: Jupiter's radiation belts

R.J. Sault[1], **T. Oosterloo**[2], **G.A. Dulk**[3,4], **and Y. Leblanc**[3]

[1] Australia Telescope National Facility, CSIRO, P.O. Box 76, Epping, N.S.W. 2121, Australia
[2] Istituto di Fisica Cosmica del CNR, Via Bassini 15, I-20133 Milano, Italy
[3] CNRS–URA 264, DESPA, Observatoire de Paris, F-92195 Meudon, France
[4] Department of Astrophysical, Planetary and Atmospheric Sciences, University of Colorado, Boulder, CO 80309, USA

Received 5 December 1996 / Accepted 17 February 1997

Abstract. For an object where the emission is optically thin, it is shown that the visibility measured by an interferometer is a sample of the three-dimensional Fourier transform of the object. If the object rotates, then it is possible to sample this three-dimensional Fourier space adequately, and so reconstruct the object in three dimensions. Using this principle, reconstructions of Jupiter's synchrotron radiation belts can be formed. This paper considers the principle and practice of this reconstruction process.

Key words: planets and satellites: individual: Jupiter – techniques: interferometric – methods: data analysis

1. Introduction

Astronomical observations normally produce images which are projections of the true sources onto the celestial sphere. Losing the three-dimensionality makes interpreting the results more difficult. Indeed, going from three to two dimensions loses information, in much the same way as going from a two-dimensional image to a one-dimensional scan. Clearly, interpretation is much easier if the object can be 'seen' in all its spatial dimensions.

Although an assumption of circular or spherical symmetry is often used to invert the projection operation, true astronomical three-dimensional reconstructions are comparatively rare. To date, the Sun is probably the only object where true three-dimensional reconstructions exist. These have been achieved using a number of techniques: helioseismology (e.g. Christensen-Dalsgaard et al. 1990; Kosovichev 1996) gives information on the interior, whereas radio stereoscopy and tomography from visible to x-ray wavelengths have been used to reconstruct coronal characteristics (e.g. Altschuler 1979; Aschwanden 1995). Tomographic principles have also been used to reconstruct (albeit in two dimensions) accretion disks (Horne 1985; Marsh & Horne 1988). While "three-dimensional reconstructions" of the planets can be readily achieved by re-projecting onto a spheroid, this is really "two dimensional" in that it gives a brightness distribution on a surface.

In this paper, we present a new radio interferometric technique to form a true three-dimensional reconstruction of Jupiter's synchrotron radiation belts (van Allen belts). In Sects. 2 and 3, we show that the visibility measured by a radio interferometer is a sample in a *three-dimensional* Fourier space, and so can be inverted to produce a three-dimensional reconstruction. Sects. 4 to 6 demonstrate that this can be a practical technique. To be so relies on the rotation of the radiation belts with Jupiter and on the belts' being optically thin. The final three sections deal with some limitations, an example, and some conclusions of the Jupiter imaging.

This paper concentrates on the technique of three-dimensional reconstruction. Our experience with the technique is based on observations with the Australia Telescope Compact Array (ATCA) (Australia Telescope 1992) made at λ = 22 and 13 cm in 1995 July. Analysis and interpretation of these observations is described elsewhere (Leblanc et al. 1996; Dulk et al. 1996).

2. An intuitive approach

In conventional interferometric imaging, the relationship between the projected sky and the visibility function (the quantity measured by an interferometer) is given by the van Cittert-Zernike equation (e.g. Clark 1989). This is essentially a two-dimensional Fourier transform relationship. That is, the visibility measured by an interferometer is a sample of the two-dimensional Fourier transform of the projected sky. By using Earth rotation and interferometer arrays, a reasonable sampling of the Fourier plane is possible, and a Fourier transform can be used to form an image of the projected sky.

Soon after radio interferometric imaging became a practical technique, Berge (1966) formed a two-dimensional image of Jupiter's radiation belts, assuming a symmetry about a tilted dipolar magnetic field. Branson (1968) was the first to undertake interferometric observations which made some discrimina-

Send offprint requests to: R.J. Sault

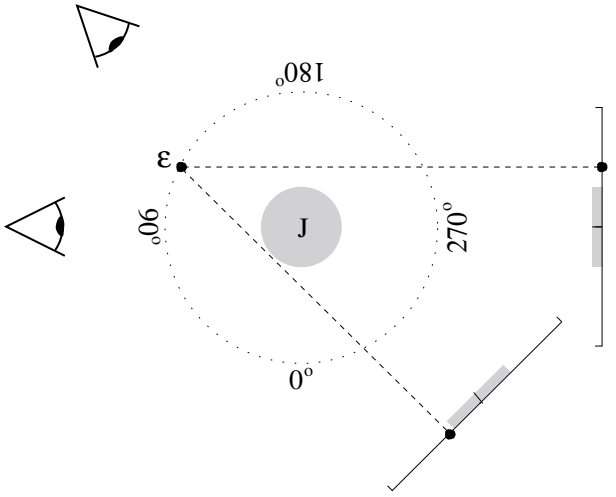

Fig. 1. This is a sketch of tomographic technique. The projected Jovicentric position of an emitter, $\mathscr{E}$, changes with the viewing aspect. For a point source, two viewing aspects are sufficient to invert the projection operation.

tion between different rotational aspects of the belts. By the late 1970s and early 1980s, high-quality images of the different rotational aspects were being produced by de Pater and co-workers (e.g. de Pater 1980; de Pater & Jaffe 1984). Given views at the different rotation aspects, and assuming that the emission is optically thin, it is apparent that techniques similar to medical x-ray tomography (e.g. Bracewell 1995) could generate a three-dimensional reconstruction. A sketch of a tomographic reconstruction is given in Fig. 1: the projected Jovicentric position of an emitter, $\mathscr{E}$, changes as the viewing angle of the observer changes. For a point-source emitter, two viewing aspects are sufficient to determine the position of the emitter. For more complex emitters, more viewing aspects are needed.

One approach to tomographic reconstruction is to use the projection-slice theorem (Bracewell 1995). This theorem states that a projection operator in the image domain is equivalent to a slice operator in the Fourier domain. As the images at different rotational aspects are projections, their two-dimensional Fourier transforms are slices of the three-dimensional Fourier transform of the radiation belts – different images correspond to different slices. As the images are derived from Fourier data initially, it is apparent that the argument can be taken a step further: the visibility measured by an interferometer is a sample of a three-dimensional Fourier space.

3. The imaging equation

To derive this relationship more formally, we parallel the approach of Clark (1989 – see this reference for more details than are given here), and derive the van Cittert-Zernike equation for a three-dimensional object.

By Huygens' principle, the emission, E, received by an observer at $\boldsymbol{r}$ from the emitter, $\mathscr{E}$, at $\boldsymbol{R}+\boldsymbol{x}$, is

$$E(\boldsymbol{R}+\boldsymbol{x},\boldsymbol{r}) = \mathscr{E}(\boldsymbol{R}+\boldsymbol{x})\frac{\exp(i2\pi|\boldsymbol{R}+\boldsymbol{x}-\boldsymbol{r}|/\lambda)}{|\boldsymbol{R}+\boldsymbol{x}-\boldsymbol{r}|}. \quad (1)$$

Here $\boldsymbol{R}$ is the position vector to the centre of the object of interest, and $\boldsymbol{x}$ is the position vector of the emitter within the object. In using Huygens' principle, we have assumed that the emission is isotropic and that the path to the observer is optically thin. We reconsider these assumptions later.

The visibility function, V, is the complex correlation of the emission received at two locations $\boldsymbol{r_1}$ and $\boldsymbol{r_2}$:

$$V = \int I(\boldsymbol{x}) \quad \frac{\exp(i2\pi|\boldsymbol{R}+\boldsymbol{x}-\boldsymbol{r_1}|/\lambda)}{|\boldsymbol{R}+\boldsymbol{x}-\boldsymbol{r_1}|} \frac{\exp(-i2\pi|\boldsymbol{R}+\boldsymbol{x}-\boldsymbol{r_2}|/\lambda)}{|\boldsymbol{R}+\boldsymbol{x}-\boldsymbol{r_2}|}\, d\boldsymbol{x}, \quad (2)$$

where

$$I(\boldsymbol{x}) = \langle|\mathscr{E}(\boldsymbol{R}+\boldsymbol{x})|^2\rangle. \quad (3)$$

The integration is over the volume of the emitting region. This result assumes that the emission is spatially incoherent and is quasi-monochromatic.

We can expand the expressions for the phase terms in a Taylor series. For this, it is convenient to select the origin to be near the observer so that $|\boldsymbol{r}| \ll |\boldsymbol{R}|$. In the Taylor expansion, many phase terms cancel and high-order terms can be discarded (this is a far-field approximation). We neglect terms smaller than of order $|\boldsymbol{r}||\boldsymbol{x}|/|\boldsymbol{R}|$. Additionally we assume that $|\boldsymbol{r}| \ll |\boldsymbol{x}|$ (i.e. Earth-based baselines are small compared with the size of the object being observed). Note that some terms which are second-order in the Taylor expansion are significant and must be retained. Defining the baseline vector, $\boldsymbol{\Delta r} = \boldsymbol{r_1} - \boldsymbol{r_2}$, the distance to the source, $R = |\boldsymbol{R}|$, and the unit vector in the direction of the source, $\hat{\boldsymbol{n}} = \boldsymbol{R}/R$, Eq. (2) simplifies to

$$V = \frac{1}{R^2}\int I(\boldsymbol{x}) \exp\left(-i2\pi\frac{L}{\lambda}\right) d\boldsymbol{x}, \quad (4)$$

where L is the excess path length,

$$L = \hat{\boldsymbol{n}}\cdot\boldsymbol{\Delta r} + \frac{\boldsymbol{x}\cdot\boldsymbol{\Delta r} - (\hat{\boldsymbol{n}}\cdot\boldsymbol{x})(\hat{\boldsymbol{n}}\cdot\boldsymbol{\Delta r})}{R}. \quad (5)$$

The phase terms neglected in the Taylor expansion are no larger than $\pi b^2/(\lambda R)$ (where b is the baseline length). For $\lambda = 22$ cm and $R = 5$ AU, a 1° phase error will occur for a baseline of about 30 km. Special phasing of the interferometer array can be used to eliminate some of the neglected terms, and so extend the range of the approximation to considerably larger baselines.

Eqs. (4) and (5) require further modification:

– In practice, the quasi-monochromatic assumption is not a good one for interferometers. Indeed, monochromaticity and spatial incoherence are mutually inconsistent. To maintain correlation, an extra time delay must be inserted into the

signal paths to align the wavefronts received at the two interferometer elements – this is the so-called "delay-tracking" term. In our notation, this reduces the excess path length, L, by $\hat{\boldsymbol{n}} \cdot \boldsymbol{\Delta r}$.

– By convention, astronomers normalize the brightness of Jupiter to a standard distance, $R_0 = 4.04$ AU. Consequently, we define $I_0(\boldsymbol{x}) = I(\boldsymbol{x})/R_0^2$.
– As a matter of notation, let the source position vector be $\boldsymbol{x} = (x, y, z)$ and define the *projected* baseline vector

$$(u, v, w) = \boldsymbol{\Delta r} - (\hat{\boldsymbol{n}} \cdot \boldsymbol{\Delta r})\hat{\boldsymbol{n}}. \quad (6)$$

With these changes, Eq. (4) simplifies to

$$V(u,v,w) = \left(\frac{R_0}{R}\right)^2 \int I_0(x,y,z) \exp\left(-i2\pi(xu + yv + zw)/(\lambda R)\right) dx\, dy\, dz. \quad (7)$$

We will call this the imaging equation.

The imaging equation represents a Fourier pair:

$$\left(\frac{R}{R_0}\right)^2 V(u,v,w) \Longleftrightarrow I_0(x,y,z). \quad (8)$$

Apart from some scale factors, the projected baseline vector (u, v, w), and the source position vector (x, y, z) form conjugate coordinate systems. If an adequate sampling of the Fourier space can be achieved, a true three-dimensional reconstruction is possible.

One aspect that has been omitted from the imaging equation is the "primary beam" response from individual interferometer elements. For normal synthesis, the primary beam is well approximated as being circularly symmetric. Thus for a telescope with an alt-az mount, the effect of the primary beam is constant over the course of a long synthesis. Such an assumption cannot be applied to three-dimensional reconstruction – the effective "primary beam" response is cylindrical and it rotates with the source. Provided we restrict ourselves to objects that are much smaller than the primary beam, the primary beam response can be ignored.

4. Sampling the Fourier space

As the radiation belts are 'frozen' into Jupiter's magnetic field, they rotate at the same rate as Jupiter's dynamo – it is only as a result of this rotation that it is possible to sample the three-dimensional Fourier space [1]. Because (x, y, z) and (u, v, w) are defined in the frame of the source, they rotate with the source. As a result, the Fourier sampling changes as the source rotates. This is a generalisation of conventional interferometry which uses Earth rotation synthesis. With a rotation period of 9^h55^m, Jupiter is reasonably matched to the Earth's rotation period, the capacity of modern interferometers and the patience of the observer.

[1] Strictly, to sample the three-dimensional Fourier space, the rotation axis of the source must not be parallel to the line of sight. With Jupiter the geometry is near optimum, as the rotation axis and line of sight are within a few degrees of being orthogonal.

Consider the definition of the *projected* baseline vector, (u, v, w), in Eq. (6). This represents the baseline vector projected onto a plane normal to the direction of the source – a displacement of an interferometer element in the direction of the source provides no additional information. This has an analogy in normal two-dimensional imaging: the component of the baseline vector in the direction of the source (which is conventionally defined to be the w axis) does not enter into the Fourier relationship (e.g. Thompson et al. 1986). It is possible to take this parallel further: normal two-dimensional imaging can be interpreted as a special case of three-dimensional reconstruction. With a normal observation where the source does not rotate, the Fourier samples are confined to a plane. Indeed, when the w-axis is in the direction of the source, this is the $u - v$ plane. Inverting such data with a three-dimensional Fourier transform would result in a reconstruction with no resolution in the depth direction.

Because the Earth-Jupiter distance, R, appears in the phase term of the imaging equation, variation in this distance also results in different sampling in the Fourier space. This is similar to multi-frequency synthesis (Conway et al. 1990; Sault & Wieringa 1994) which varies λ. Varying either λ or R results in a scaling of the effective baseline vector. For Jupiter, R varies between about 4 and 6 AU within 13 months. Other changes in Earth-Jupiter geometry, caused by Jupiter's 12 yr revolution around the Sun, also modify the Fourier space sampling.

For our observations with the ATCA, which consists of 6 antennas on a 6 km east-west track, ten 12 h days' observing gives a modest sampling of the three-dimensional Fourier space of Jupiter. For 10 days' observing, the best Fourier coverage occurs when the observing time is split into two 5 day sessions separated by 5 days. This is because of the relative rotation rates of Jupiter (9.9 h) and the Earth (23.9 h). As these almost beat with a 5 day period, in 10 consecutive days of observing, the second 5 days would produce only marginally different Fourier samples. Our observations with the ATCA also made modest use of multi-frequency synthesis. Variation in R over 15 days does not significantly contribute to the coverage. Examples of the Fourier coverage of our observations are given in Fig. 2.

For an array with good instantaneous two-dimensional coverage (e.g. the VLA), an observation of a single rotation of Jupiter would be adequate to produce a good three-dimensional Fourier coverage.

5. Geometry

In several places in the reconstruction process, we need to model various geometric aspects of Jupiter and its relationship to the Earth. Our geometric model is based on Hilton's (1992) physical ephemerides, the rotation elements defined by System III (1965) (Seidelmann & Divine 1977) and orbital ephemerides derived from Simon et al. (1994). Although these orbital ephemerides are not of the highest precision, their accuracy is more than adequate for the geometric requirements. All geometry is corrected for light travel time.

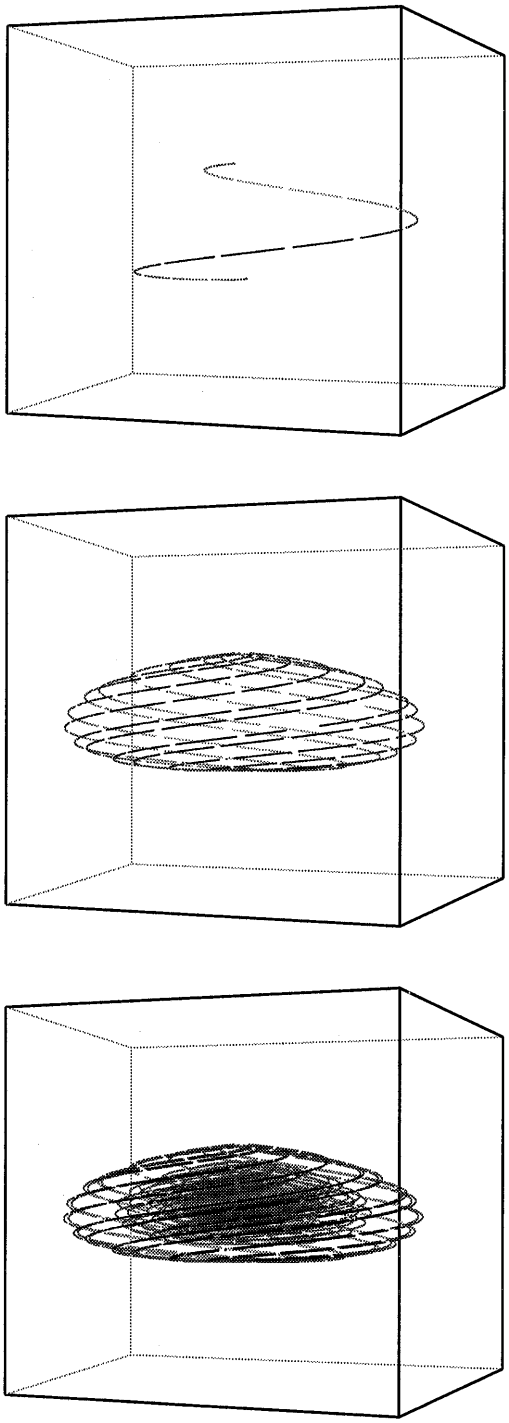

Fig. 2. Three-dimensional Fourier space coverage resulting from ATCA observations. Width, depth and height correspond to the Fourier transforms axes of the spatial x, y and z dimensions. The shade of the points goes from black to grey with increasing depth. Each panel shows $\pm 62 \times 10^3$ wavelengths along each axis for 13 cm observations. The top panel shows the coverage for a 12 h observation with a single baseline. The middle panel shows the coverage from ten 12 h days' observing with the same baseline as the top panel. The bottom panel gives the coverage achieved from a 10-day run with all 15 ATCA baselines. The figure does not include the extra coverage gained from multi-frequency synthesis, nor from the conjugate samples.

6. The reconstruction process

To implement three-dimensional reconstruction, we have generally used extensions to the normal synthesis imaging techniques (e.g. see Thompson et al. 1986). For example, we use the so-called 'grid-and-FFT' approach to form an 'image' from the visibility data. In this approach, an image is formed by using an FFT after the visibilities have been convolved onto a grid. We use a prolate-spheroidal function (Schwab 1984b) for the gridding function. For a given gridding function, the grid-correction required in three-dimensional reconstructions is that required in two-dimensions raised to the three-halves power. Thus the grid-correction factor is normally significantly larger in three-dimensional reconstructions: Schwab's cautions on the effects of roundoff error on the grid-correction step become very relevant.

As with conventional two-dimensional synthesis, deconvolution is essential. In our approach, the imaging and deconvolution steps are bound together in an "MX-like" CLEAN algorithm (see Högbom 1974, or the review by Cornwell & Braun 1989). CLEAN decomposes the sky into a collection of point sources using an iterative process with two basic steps: it first estimates the flux density and position of a point source and it then subtracts this source. Provided the grid used is fine enough (typically a third of the intrinsic resolution of the observation) CLEAN continues to work tolerably well even for extended sources. Whereas the iterations of the classical CLEAN algorithm subtracts the point sources in the image domain, the so-called MX algorithm (developed by W.D. Cotton and F.R. Schwab, as reported in Schwab 1984a) subtracts the point sources directly from the visibility data. In this way, the MX algorithm avoids some artifacts resulting from approximations implicit in the grid-and-FFT approach.

An MX CLEAN is a form of an iterative-refinement algorithm. It uses a "crude inverse" operation (a conventional grid-and-FFT technique followed by a partial CLEAN) to estimate a model of the true sky, and then this model is used with an "accurate forward" operation to predict the visibilities that would result from such an object. The difference between the observed and model visibilities are then fed back into the same process. Because the deconvolution is iterative, the errors in the "crude inverse" step are nullified in the "accurate forward" step. In this way, the model is incrementally improved by successive steps.

By using an iterative-refinement approach in our three-dimensional reconstruction technique, we can relax the "optically thin" assumption. As mentioned in Sect. 3, the optically thin assumption is critical in deriving the imaging equation. Whereas this is a good assumption for the radiation belts, the disk of Jupiter is opaque and it shadows part of the radiation belts. The effect is not excessively severe – at any given time about 20% of the radiation belt emission is shadowed by Jupiter's disk.

In our MX approach, the "crude inverse" operation (grid-and-FFT) ignores shadowing. However, in the "accurate forward" operation, where the model visibilities are generated from the collection of CLEAN point sources, we determine if a par-

ticular point source was shadowed when a particular visibility was measured. If it was shadowed, it does not contribute to the measured visibility. In this way, the iterative-refinement deconvolution compensates for the shadowing ignored in the imaging equation.

In addition to shadowing, the disk emits thermal radiation. This emission cannot be treated in the same way as the radiation belts. For an opaque emitter, shadowing cannot be neglected in the imaging equation in the way we have done. As we are not interested in the disk emission, we simply subtract it directly from the visibility data before we do any reconstruction. We model the emission as a black-body radiator with a temperature of 350 and 280 K at 22 and 13 cm respectively. We do not model any limb darkening, nor do the data show evidence for it. We have confidence in this simple model: it is effective at representing the visibility data on the longer baselines, where the emission from the radiation belts is resolved out (limb darkening would be apparent in these longer baselines).

In a similar way, other sources which do not obey the imaging equation can be subtracted from the visibility data before reconstruction. While emission from Jupiter's satellites is too weak to be of concern (e.g. de Pater et al. 1984), background radio sources can have a deleterious effect on the reconstructions. At 22 cm, it is normal to have several sources of up to about 100 mJy within the $35'$ primary beam of the ATCA. Because background sources move at the sidereal, rather than Jovian, rate, and because they do not obey the imaging equation, they are smeared out by the reconstruction process, and appear as rather unusual artifacts. However, as the background sources are usually simple point sources and rarely complex, it is straightforward to locate, model and subtract them from the visibility data.

7. Beaming and time variability

The imaging equation assumes that the emission is isotropic (or at least that the apparent emission of a region is independent of Jupiter's rotation aspect). The emission from the radiation belts is caused by relativistic electrons gyrating in Jupiter's magnetic field. The emission from an electron is significantly beamed and the electron pitch-angle distribution is far from isotropic (e.g. Roberts & Komesaroff 1965). This, combined with the misalignment of rotation and magnetic axes (they differ by 10°) means that the apparent emission from a region is modulated by the rotation of Jupiter. The effect is quite significant: Leblanc et al. (1996) show that the apparent emission of some regions varies as much as $\pm 20\%$. The modulation of most regions, however, is more modest.

To date, we have ignored this modulation in our reconstructions; this results in errors. With good Fourier space coverage, however, the resulting errors are not as significant as might be expected. Our reconstructions represent an average of the apparent emission, with the averaging being taken over the rotation aspects where the emitting region is not shadowed. Because the variation of the apparent emission is not modelled in the deconvolution process, deconvolution errors will ultimately limit the quality of our reconstructions. Given the Fourier space coverage for our experiments and for a $\pm 20\%$ modulation in the apparent emission, point-source simulations suggest a dynamic range limit of 1200 and a fidelity limit of 90. As the quality of our reconstructions is limited well below this by the modest Fourier coverage and other deconvolution errors, ignoring beaming is reasonable.

We are actively investigating methods of modelling beaming in our reconstruction process. Dulk et al. (1996) show that simple models of the magnetic field are quite effective at modelling beaming. We intend to include such a model in the deconvolution process, in a similar way to shadowing.

Another assumption of rotation synthesis (either Jovian or Earth rotation) is that there is no intrinsic change in the source during the observation (15 days in our case). Although the processes involved in the drift, diffusion and loss of the electrons are complicated (de Pater 1981), if these are in equilibrium then obviously variability is not expected. Although short-term (weeks) variability has been rumoured, no convincing results have been published (Hood 1993) except at the time of the collision of Jupiter and Comet Shoemaker-Levy 9 (de Pater et al. 1995; Dulk et al. 1995; Leblanc & Dulk 1995). There is, however, an undisputed long-term ($\sim$ 12 yr) variability (Bolton et al. 1989; Hood 1993). Apart from normalizing the reconstruction to R_0 = 4.04 AU (eliminating the $1/R^2$ dependence), our reconstruction technique does not model any time variability of the radiation belts.

8. An example

Fig. 3 gives different aspects of a reconstruction of the radiation belts. See Leblanc et al. (1996) for more details. Although the radiation belts are optically thin, they are represented here with a technique which approximates an intensity contour. An animation of the reconstructed radiation belts is available from `http://www.atnf.csiro.au/~rsault/Jupiter`.

The effect limiting these reconstructions is the modest Fourier space coverage. Particular at λ = 13 cm, the radiation belts are resolved out on the longer baselines in our observations.

9. Conclusions

We have described a new technique which can produce true three-dimensional reconstructions from radio-interferometric observations, e.g. of Jupiter's radiation belts. One of the strengths of this reconstruction technique is that it is only weakly dependent on models. Basically it relies on only some well-known Jovian geometry as well as the assumption that the radiation belts are optically thin.

Using the results of this technique, we are able, for the first time, to make use of the normal three-dimensional perception. This allows us to see Jupiter in a new light – it greatly simplifies the task of interpreting our data. Use of the technique on Jovian observations is described in Leblanc et al. (1996) and Dulk et al. (1996).

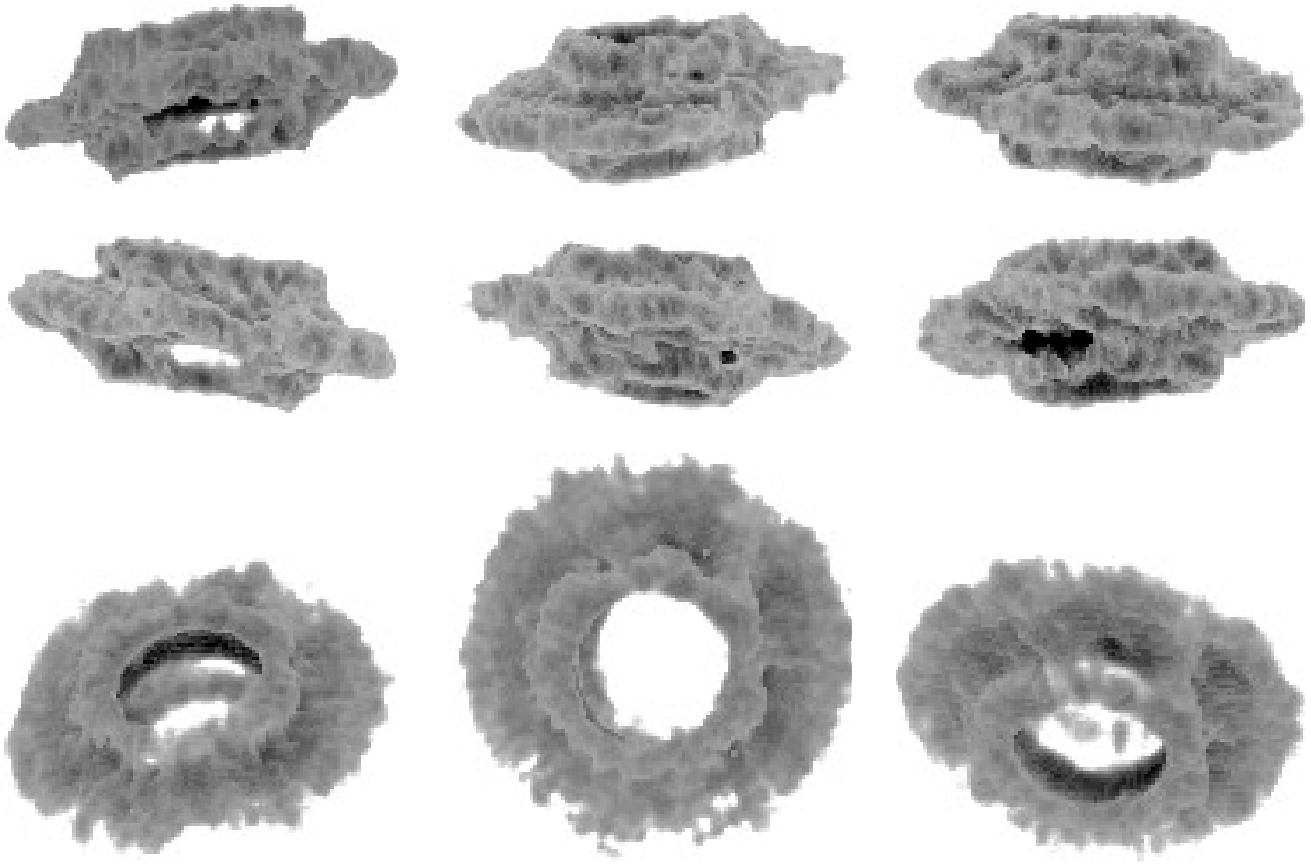

Fig. 3. Three-dimensional reconstructions of Jupiter's radiation belts at 13 cm. These are derived from ten 12 h days of observing. The first six reconstructions correspond to Jupiter viewed with a central meridian longitude of 90° to 330° in increments of 60°. The last three correspond to a central meridian longitude of 90°, but viewed at an angle of 40°, 90° (i.e. the north pole) and 130° to the ecliptic. The planet's thermal emission has been subtracted before the reconstruction process.

A natural question is: what other sources are candidates for this three-dimensional reconstruction technique? A suitable object must be large enough to resolve, and have a rotation period which is not excessively long (i.e. much shorter than the lifetime of an astronomer!). This limits the technique to comparatively nearby objects. It is not apparent that there are any candidates outside the solar system, although VLBI techniques may soon reveal some resolved, rotating stellar sources. Even within the solar system, the candidates are few: Jupiter is the only planet that has appreciable synchrotron emission (van Allen 1996). The Sun's corona is more promising, particularly in its polar regions. However, the slow solar rotation, particularly when the Sun's variability is considered, makes it a more difficult object. Jupiter's radiation belts are easily the best candidates for the technique.

Acknowledgements. We thank R.D. Ekers for his continuing support and enthusiasm for this project. R.E. Gooch has helped us considerably in the visualisation of our reconstructions.

References

Altschuler M.D., 1979, in G.T. Herman (ed.), Image Reconstruction from projections, Topics in Applied Physics, Springer-Verlag, Berlin, 32, 105

Aschwanden M.J., 1995, in A.O. Benz and A. Krüger (eds). Lecture Notes of Physics, Springer-Verlag, 444, 13

Australia Telescope, 1992, J. Electr. Electron. Eng. Aust., Special Issue, 12, no. 2

Berge G.L., 1966, ApJ, 146, 767

Bolton S.J., Gulkis S., Klein M.J., de Pater I., Thompson T.J., 1989, JGR, 94, 121

Bracewell R.N., 1995, Two-dimensional imaging, Prentice-Hall, Englewood Cliffs

Branson N.J.B.A., 1968, MNRAS, 139, 155

Christensen-Dalsgaard J., Schou J., Thompson M.J., 1990, MNRAS, 242, 353

Clark B.G., 1989, in R. A. Perley, F. R. Schwab, and A. H. Bridle (eds.), Synthesis Imaging in Radio Astronomy, A.S.P. Conf. Ser., 6, 1

Conway J.E., Cornwell T.J., Wilkinson P.N., 1990, MNRAS, 246, 490

Cornwell T.J., Braun R., 1989, in R. A. Perley, F. R. Schwab, and A. H. Bridle (eds.), Synthesis Imaging in Radio Astronomy, A.S.P. Conf. Ser., 6, 167

de Pater I., 1980, A&A, 88, 175

de Pater I., 1981, JGR, 86, 3397

de Pater I., Jaffe W.J., 1984, ApJS, 54, 405

de Pater I., Brown R.A., Dickel J.R., 1984, Icarus, 57, 93

de Pater I., Heiles C., Wong M., Maddalena R.J., Bird M.K., Funke O., Neidhoefer J., Price R.M., Kesteven M., Calabretta M.,

Klein M.J., Gulkis S., Bolton S.J., Foster R.S., Sukumar S., Strom R.G., LePoole R.S., Spoelstra T., Robinson M., Hunstead R.W., Campbell-Wilson D., Ye T., Dulk G., Leblanc Y., Galopeau P., Gerard E., Lecacheux A., 1995, Science, 268, 1879
Dulk G.A., Leblanc Y., Hunstead R.W., 1995, GRL, 22, 1789
Dulk G.A., Leblanc Y., Sault R.J., Ladreiter H.P., Connerney J.E.P., 1996, to appear in A&A.
Hilton J.L., 1992, in P.K. Seidelmann (ed.) Explanatory Supplement to the Astronomical Almanac, Univ. Science Books, Mill Valley, CA, p. 383
Högbom J.A., 1974, A&AS, 15, 417
Hood L.L., 1993, JGR, 98, 5769
Horne K., 1985, MNRAS, 213, 129
Kosovichev A.G., 1996, ApJ, 461, L55
Leblanc Y., Dulk G.A., 1995, GRL, 22, 1797
Leblanc Y., Dulk G.A., Sault R.J., Hunstead R.W., 1996, to appear in A&A.
Marsh T.R., Horne K., 1988, MNRAS, 235, 269
Roberts J.A., Komesaroff M.M., 1965, Icarus, 4, 127
Sault R.J., Wieringa M.H., 1994, A&AS, 108, 585
Schwab F.R., 1984a, AJ, 89, 1076
Schwab F.R. 1984b, in J.A. Roberts (ed.), Proc. IAU/URSI Conference on Indirect Imaging, Sydney, Cambridge University Press, p. 330
Seidelmann P.K., Divine N., 1977, GRL, 4, 65
Simon J.L, Bretagnon P., Chapront J., Chapront-Touze M., Francou G., Laskar J., 1994, A&A, 282, 663
Thompson A.R., Moran J.M., Swenson G.W. Jr, 1986, Interferometry and Synthesis in Radio Astronomy, John Wiley & Sons, New York
van Allen J.A., 1996, Icarus, 122, 209

This article was processed by the author using Springer-Verlag LaTeX A&A style file *L-AA* version 3.